Microgravity Science and Technology (2021) 33: 41
https://doi.org/10.1007/s12217-021-09875-7

ORIGINAL ARTICLE

Numerical Simulations of Arm-locking for Taiji Space Gravitational Waves Detection

Hang Liu[1,2] · Yuqiong Li[1] · Gang Jin[1]

Received: 28 August 2020 / Accepted: 4 February 2021 / Published online: 3 June 2021

Abstract

The laser frequency stabilization is one of the most important key technologies for the interferometer measurement system of space gravitational waves detection. As a proposed frequency stabilization technique, the scheme of arm-locking is to convert the stability of interferometer arm-length into the stability of laser frequency. Some numerical simulations of arm-locking for Taiji mission were investigated in the paper. Meanwhile, an innovative controller consisted of a compensation filter and two-stage integrators in parallel was presented to suppress the laser frequency noise without increasing gain and prevent the high gain from suppressing the gravitational waves signal. The single arm-locking simulation results showed that the laser noise of closed loop was lower than 3.19 $\mu m/\sqrt{Hz}$@10 mHz only in the frequency range of 0.1 mHz – 0.03 Hz. But the dual arm-locking simulation results showed that the laser noise of closed loop was lower than 3.19 $\mu m/\sqrt{Hz}$@10 mHz in the full frequency range of 0.1 mHz – 1 Hz, meeting the requirement of Taiji mission. Preliminary results represented the feasibility and effectiveness of arm-locking on laser frequency stabilization for the Taiji mission.

Keyword Arm-locking · laser frequency stabilization · taiji mission · gravitational waves detection

Introduction

The Laser Interferometer Gravitational-Wave Observatory (LIGO) group first observed a transient gravitational waves (GWs) signal from a binary black hole merger in 2015 (Abbott et al. 2016a), and the group observed the GWs several times during the next few years (Abbott et al. 2016b, 2018; Scientific et al. 2017), which represents the arrival of the era of GWs detection. Besides the LIGO (Abramovici et al. 1992; Arain, Mueller 2008), the ground-based GWs detectors such as VIRGO (Acernese et al. 2010; Beker et al. 2012) and GEO 600 (Willke et al. 2002; Grote, Collaboration 2010) are sensitive to the medium and high frequency GWs, which are limited by the laser interferometer arm-length and the earth seismic noise. To complement the frequency band of ground-based GWs detectors, space-based GWs detection antennas such as LISA (Laser Interferometer Space Antenna) (Robertson, Hough 1996; Cornish 2001), DECIGO (DECi-heltz Gravitational-wave Observatory) (Kawamura et al. 2006; Ando et al. 2010), Taiji (Cyranoski 2016; Hu, Wu 2017) and Tianqin (Cyranoski 2016; Luo et al. 2016) and so on were put forward in succession, which could detect the GWs at medium–low frequencies (Pitkin et al. 2011; Gair et al. 2013). The Taiji mission was proposed by the Chinese Academy of Sciences (CAS), which would launch three spacecraft into space to observe GWs by using the methodology of heterodyne laser interference. The spacecraft will be placed in solar orbit to form an equilateral triangle with arm-length of approximately 3×10^9 m (Cyranoski 2016). According to the intensity of GWs and the arm-length of laser interferometer, the requirement of measurement sensitivity of laser interferometer reaches a few picometers levels within the frequency range of 0.1 mHz –1 Hz (Luo et al. 2020).

The frequency noise resulted from the frequency instability of the laser is the maximum noise source for the space laser interferometer. To meet the requirement of the Taiji space GWs detection, the scientific consensus is to adopt a three-step method to suppress the laser frequency noise, including Pound-Drever-Hall (PDH) technique (Black 2001), Arm-Locking (Sheard et al. 2003; Sutton, Shaddock 2008;

✉ Yuqiong Li
liyuqiong@imech.ac.cn

[1] National Microgravity Laboratory, Institute of Mechanics, Chinese Academy of Sciences, Beijing 100190, China

[2] School of Engineering Science, University of Chinese Academy of Science, Beijing 100049, China

McKenzie et al. 2009) and Time Delay Interferometer (TDI) (de Vine et al. 2010; Wang, Ni 2019). The frequency stability of laser can reach $30Hz/\sqrt{Hz}\cdot\sqrt{1+(2.8\ mHz/f)^4}$ by the PDH pre-stabilization (McKenzie et al. 2009; Luo et al. 2020). In addition, the arm-locking technology can suppress the frequency noise with two orders of magnitude, and the corresponding frequency noise is down to $0.3Hz/\sqrt{Hz}\cdot\sqrt{1+(2.8\ mHz/f)^4}$ (Danzmann et al. 2011). At last, the data processing methodology of TDI is adopted to suppress the laser frequency noise below the secondary noise, such as optical path noise, acceleration noise etc., to attain the requisite sensitivity (de Vine et al. 2010; Danzmann et al. 2011; Wang, Ni 2019). Here, only the arm-locking technique will be discussed in this paper.

Since the 2000s, various scientific research groups have investigated on arm-locking technique under the impetus of space GWs detection program. Sheard et al. was the first one to report the frequency noise suppression technology by locking to a LISA arm in 2003 (Sheard et al. 2003), however, it had inherent defects that a few nulls appear inside the LISA band, which didn't get ideal noise suppression performance due to the noise amplification near the nulls, and had start-up transients as a result of the nonzero initial error signal. To overcome the above disadvantages of single arm-locking, Sutton et al. investigated the dual arm-locking by using a linear combination of two different arm's interfering signals as error signal, which didn't have noise amplification in the LISA band and had better frequency noise suppression capability (Sutton, Shaddock 2008). Besides, various scientific research groups experimentally verified the feasibility and effectiveness of arm-locking by using the electronic phase delay (EPD) (Thorpe et al. 2005) or long fiber to produce time delay (Sheard et al. 2005). The GRACE-FO (Gravity Recovery and Climate Experiment follow-on) laser ranging interferometer provided an on-orbit demonstration for the arm-locking technique in 2016 (Thorpe, McKenzie 2016). The main subject of this paper is to better understand the effectiveness of the arm-locking on the suppression of laser frequency noise through some numerical simulations, and provide parameter guidance and support for the arm-locking technology of the Taiji mission. To achieve better arm-locking performance, an innovative controller consisted of a compensation filter and two-stage integrators in parallel is presented to suppress the laser frequency noise without increasing gain and prevent the high gain from suppressing the gravitational waves signal.

Single Arm-locking

Single Arm-locking Sensor and Controller Design

The conceptual diagram of single arm-locking is shown in Fig. 1, which was proposed by Sheard et al. in 2003 (Sheard et al. 2003). The open loop laser noises p_{ol} is the intrinsic laser noise, and the close loop laser noises p_{cl} is the laser noise after single arm-locking. The error signal φ_e is the phasemeter output, which is generated by interfering the time delay signal returned from the remote spacecraft 2 with the prompt signal. In single arm-locking system, only the phasemeter output φ_e from one interferometer arm between spacecraft 1 and spacecraft 2 will be used. The transfer function of the single arm-locking sensor from input laser noise to the phasemeter output is $H_s(s) = 1 - e^{s\tau_2}$ (Sheard et al. 2003; McKenzie et al. 2009). The magnitude response of the sensor transfer function has zero points at direct-current (DC) as well as at specific frequencies n/τ_2 known as nulls, and has multiple unit gains on both sides near each null. At these nulls the phase response has 180° phase shift from -90° to + 90°.

The noise suppression effect improves with the loop gain increasing, but the noise amplification will occur in the frequencies near each null, which places additional stability constraints on the controller design. The adopted lasers are monolithic diode-pumped solid state non-planar ring cavity Nd:YAG lasers in the Taiji mission, which are actuated by using Piezoelectric ceramic transducer (PZT) and thermal actuator to adjust the frequency. Each actuator can be represented by an integrator 1/s in the Laplace domain (Thorpe, Mueller 2005). The transfer function 1/s provides a high gain at DC and the gain decreases with a 1/s slope in the high frequency range, which is required by the practical controller bandwidth limitations. However, this transfer function provides a 90° phase lag, and the phase response becomes -180° at the nulls, which represents zero phase margin and system instability.

To solve the above question, phase compensation is necessary to improve the phase margin and the relative stability of the system. Meanwhile, the transfer function s^p can provide $p\cdot\pi/2$ phase advance. Therefore, the compensation controller can be expressed as a transfer function $G_0\cdot s^{-\alpha}$, where $0<\alpha<1$, G_0 is the gain. For example, the transfer function $s^{-1/2}$ or $s^{-2/3}$ can provide 45° or 60° phase lag, respectively. Zeros-poles model in Simulink can provide

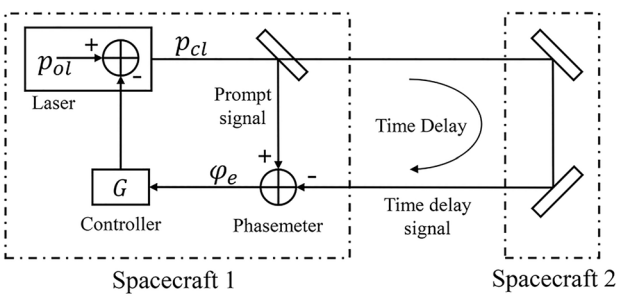

Fig. 1 Schematic of the single arm-locking system

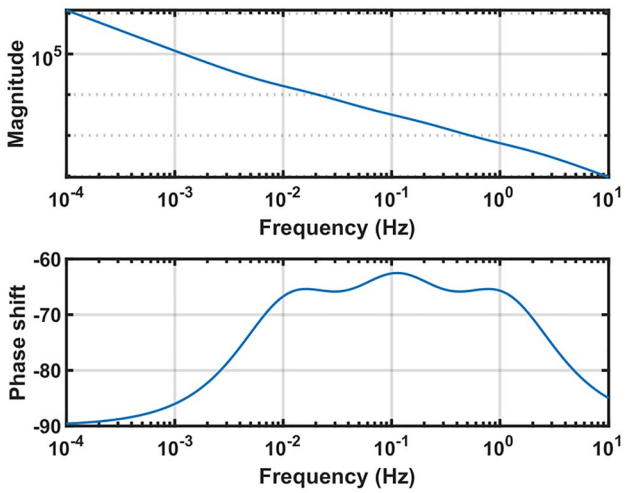

Fig. 2 The magnitude and phase response of the transfer function of compensation controller

approximate phase shift in the frequency region of $f > 1/\tau$, and the magnitude and phase response of the transfer function of the compensation controller are shown in Fig. 2. The magnitude response decreases with a $1/s$ slope and the phase response starts from a 90° phase lag at DC and keeps about 65° phase lag in the frequency region of 10 mHz – 1 Hz. The bode plot of close loop transfer function with different gains is shown in Fig. 3, and the results show that noise suppression effect improves with gain increasing and noise amplification occurs in the frequencies near each null. However, the GWs signal is identically suppressed by high gain, so it is necessary to optimize the design of the controller to reduce the gain.

The optimization method is to connect the two-stage integrator and the compensation filter in parallel. The function of the two-stage integrator is to reduce the gain, and that of the compensation filter is to improve the phase margin for frequencies above $1/\tau$. The parameters of the parallel

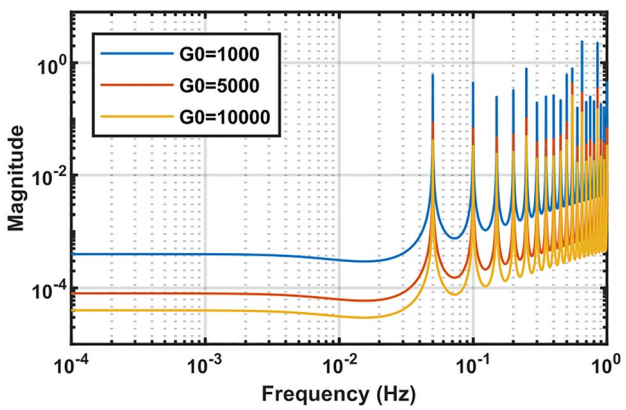

Fig. 3 The bode plot of close loop transfer function with different gains

Table 1 Parameters of the parallel controller

Compensation filter	Zeros: [-0.03 -0.3 -3 -30 -300] Poles: [-0.01 -0.1 -1 -10 -100] Gain: 10
Two-stage integrators	Transfer function: $1/s^2$
Phase margin	$\approx 50°$

controller in this simulation are shown in Table 1 and the relevant bode plot is revealed in Fig. 4. The magnitude of the transfer function of the controller decreases with $1/s^2$ slope in the frequency region of $f < 1/\tau$ to suppress the low frequency noise and has a about $1/s^{1/2}$ slope in the frequency region of $f > 1/\tau$. The phase response starts from a 180° phase lag at DC and keeps about 50° phase margin inside the frequency range of 10 mHz – 10 Hz. The close loop magnitude response of single arm-locking with the optimized controller is shown in Fig. 5, where the light transmitting time is 20 s. Meanwhile, the gain of the compensation filter in this controller has $G_1 = 10$ and the gain of the two-stage integrator is 1. Compared with the optimized controller, the filter controller shown in Fig. 3 should have a gain of $G_0 = 1000$ to achieve similar noise suppression capability. Therefore, the optimized controller consisted of a compensation filter and two-stage integrators in parallel adopted in the paper can suppress the laser frequency noise without increasing gain and prevent the high gain from suppressing the gravitational waves signal.

Numerical Simulation

Based on the above description, a numerical simulation was performed. Fig. 6 shows the Simulink model diagram of the single arm-locking system and the important

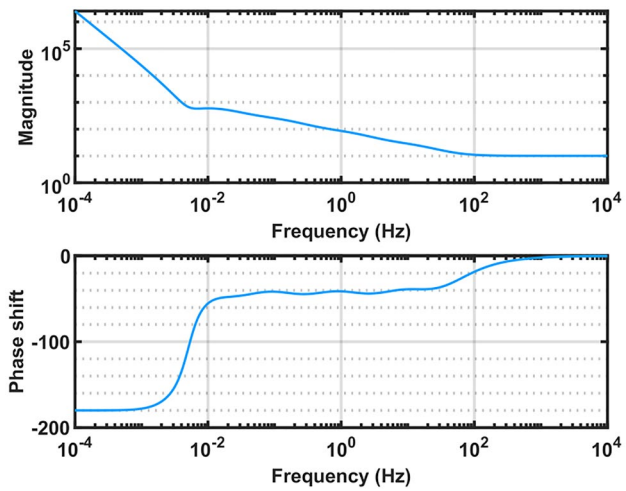

Fig. 4 The bode plot of the controller transfer function

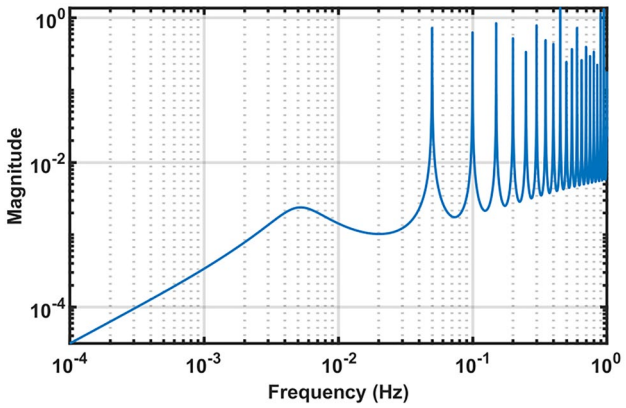

Fig. 5 An example of the close loop magnitude response of single arm-locking

parameter values used for the time domain simulation are listed in Table 2. In the whole model loop the variable is the displacement. The laser noise of close loop is a combination of the intrinsic laser noise of open loop δL_l, and the control signal provided by the arm-locking controller. The time delay blocks represent the light travel time between spacecraft 1 and spacecraft 2, which is $\tau_{12}=\tau_{21}=3\times10^9/3\times10^8=10$ s. The photo-detector is expressed as a differencing operation, where δL_s is shot noise contribution due to the low light power of the beam and δL_r is readout noise. Then, the output signal of the photo-detector measured by the phasemeter introduces a clock noise δL_c resulted from the fluctuations of the ultra-stable oscillator (USO). At last, the phasemeter output is filtered by the filter controller and

Table 2 Parameter values for the time domain simulation

Simulation Parameter	Value
Time delay $\tau_{12}=\tau_{21}$	10 s
Gian k_1	10
Gian k_2	6 000
Ramp signal slope	0.001
Ramp signal start time	20 s
Simulation time	11 000 s

feedback controls the laser. The filter controller on both spacecraft consists of a compensation filter and two-stage integrators in parallel. Meanwhile, the bode plot of controller on spacecraft 1 is shown in Fig. 4, and the gain of controller on spacecraft 2 is required to has $k_2>>1$ by the phase-locking loop (McKenzie et al. 2009; Danzmann et al. 2011). It is also worth noting that the role of the multiplier is to control the start time of feedback and reduce the turn on transients. To get the amplitude spectral density (ASD) of the laser noise before and after single arm-locking in the frequency region of 0.1 mHz – 1 Hz, the simulation time needs at least 10 000 s (Tröbs, Heinzel 2006).

Noise Levels

To make the simulation close to the actual conditions, various noise sources that exist in the Taiji mission must be considered, such as laser frequency noise, shot noise, clock noise and readout noise.

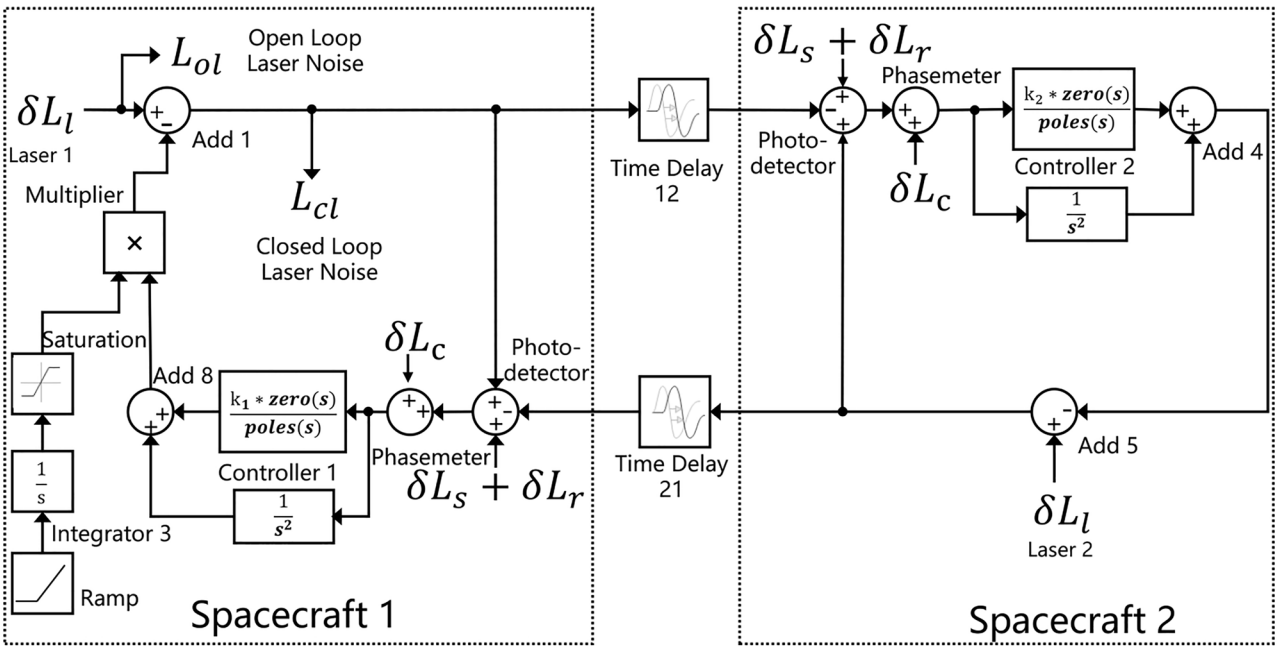

Fig. 6 The Simulink model of single arm-locking

The laser frequency noise δf after pre-stabilization is $30Hz/\sqrt{Hz} \cdot \sqrt{1+(2.8\ mHz/f)^4}$, and it can be converted into the displacement noise δL by the following formula (Danzmann et al. 2011):

$$\delta L = \Delta L \frac{\delta f}{f} \tag{1}$$

where f is the laser frequency, and $\Delta L = 3 \times 10^9$ m is the arm length of Taiji mission. Form Eq. (1), the calculated laser displacement noise δL_l is $3.19 \times 10^{-4} m/\sqrt{Hz} \cdot \sqrt{1+(2.8\ mHz/f)^4}$.

Shot noise is caused by the fluctuation in the number of photons and has a displacement noise spectrum of (Danzmann et al. 2011):

$$\delta L_S = \sqrt{\frac{\hbar c}{2\pi} \cdot \frac{\lambda}{P_{rec}}} \tag{2}$$

where $\hbar$ is the reduced Plank constant, c is speed of light, λ is the wavelength of laser and $P_{rec} \approx 100pW$ is the received power. For these numbers, the calculated shot noise is 7.3 pm/$\sqrt{\text{Hz}}$.

The displacement noise caused by the clock noise δL_c is proportional to the stability of the USO and the frequency of heterodyne signal f_h, which is given by (Danzmann et al. 2011):

$$\delta L_c = \delta t \cdot f_h \cdot \lambda \tag{3}$$

where $f_h = 20$ mHz, δt is the stability of USO. At present, the free running USO has a stability of 8×10^{-12} s/$\sqrt{\text{Hz}}$@ 1 Hz to 8×10^{-10} s/$\sqrt{\text{Hz}}$@ 10 mHz for periods of 1 s to 100 s, the free running stability of USO δt is about 8×10^{-12} Hz/f · s/$\sqrt{\text{Hz}}$. From Eq. (3), the calculated clock noise is 0.17 nm/f · Hz/$\sqrt{\text{Hz}}$.

Readout noise, including dark current noise, quadrant non-uniformity noise, crosstalk noise between quadrants, etc., is require to lower than $3.16pm/\sqrt{Hz} \cdot \sqrt{1+(2.8\ mHz/f)^4}$ in the frequency range of 0.1 mHz to 1 Hz (Dong et al. 2016).

Simulated Results

Since the simulation will run in a time series, the above-mentioned four different noises given by smooth noises function must be converted into time domain data with random characteristics. Dong et al. proposed a time domain noise generation algorithm based on inverse Fourier transform (Dong et al. 2016). The noises were introduced in simulation by using this algorithm.

To verify the validity of the generated time domain noises data and analyze the effect of the noise levels on the sensitivity of single arm-locking system, the ASD of the above noises have been calculated and compared with each other.

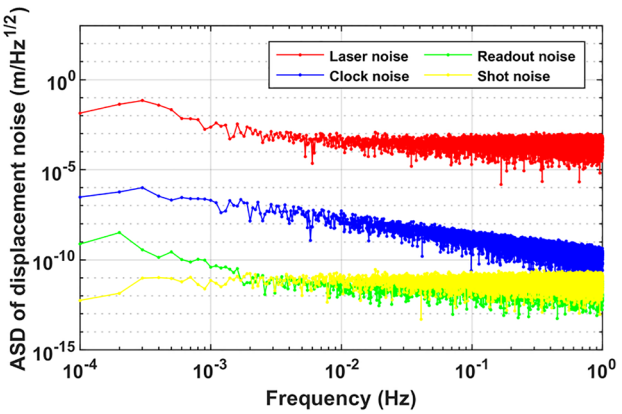

Fig.7 The noise levels of the arm-locking system

As shown in Fig. 7, the arm-locking sensitivity is dominated by laser noise, with the other noise sources being nearly four orders of magnitude smaller.

When the single arm-locking simulation began, the open loop and closed loop laser displacement noises were both respectively measured for 11 000 s, and only the last 10 000 s of data was retained to reduce the effect of the turn on transient. It is necessary to eliminate the initial unstable state data caused by the initial non-zero feedback signal value, otherwise a distortion of laser noise will be caused. Fig. 8 shows the ASD of the laser displacement noise before and after single arm-locking, where the blue trace represents the open loop laser noise and the red trace represents the closed loop laser noise. It can be concluded that it is possible to suppress the laser frequency noise with 2 orders of magnitude in frequencies below 1/τ ($\tau = \tau_{12} + \tau_{21} = 20$ s) and excess noise occurs at nulls frequencies $f = n/\tau$, as expected.

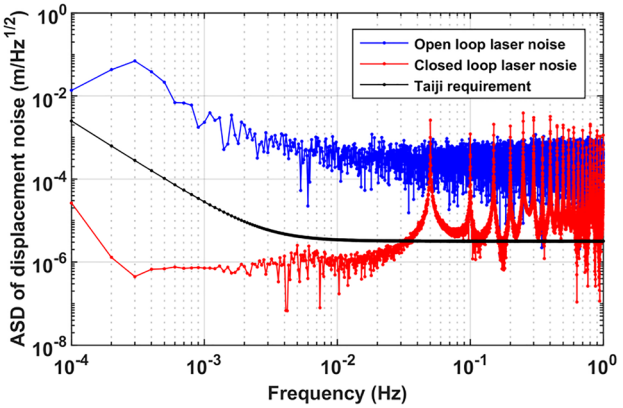

Fig. 8 The ASD of the laser noise before and after single arm-locking

Dual Arm-locking

Dual Arm-locking Sensors and Controller Design

To overcome the disadvantages of single arm-locking, Sutton et al. investigated the dual arm-locking by using a linear combination of two different arm's interfering signals to estimate the instantaneous phase information as error signal, which didn't have noise amplification in the LISA band and had better frequency noise suppression capability (Sutton, Shaddock 2008). Under the most circumstances, except for some certain short periods, the lengths of two different arms are different, so the respective light propagation times and the frequencies of nulls are also different (Hughes 2008). For these reasons, dual arm-locking takes advantage of the arm-length mismatch to eliminate the nulls in the frequency range of 0.1 mHz – 1 Hz (Sutton, Shaddock 2008). By the Laplace transform, the transfer function of dual arm-locking sensor is given by $H_d(\omega) = 2\left[1 - \left(\cos(\Delta\tau\omega) - E(\omega)\cdot \sin c(\Delta\tau\omega)e^{-i\bar{\tau}\omega}\right)\right]$, where $\Delta\tau = \left(\tau_2 - \tau_3\right)/2$, $\bar{\tau} = \left(\tau_2 + \tau_3\right)/2$, τ_2 and τ_3 are the light travel time of different arms, $E(\omega) = 1/(1 + i\omega/5\pi)$ is a low pass filter with a pole around $1/2\Delta\tau$ (Sutton, Shaddock 2008). This sensor transfer function indicates that the magnitude response is almost flat at low frequencies ($f << 1/\Delta\tau$) and the low pass filter ensures the common arm dominates with attenuating the differential arm signal at high frequencies ($f > 1/\Delta\tau$).

Numerical Simulation

Fig. 9 shows the Simulink model diagram of the dual arm-locking system and the important parameter values used for the time domain simulation are listed in Table 3. The laser noise of close loop is a combination of the intrinsic laser noise of open loop δL_l, and the control signal provided by the arm-locking controller. The time delay blocks represent two different arm's light travel time, which are $\tau_2 = 20$ s and $\tau_3 = 20.2$ s, the arm length mismatch is ~ 1% (Hughes 2008). The photo-detector is expressed as a differencing operation, where δL_s is shot noise contribution due to the low light power of the beam and δL_r is readout noise. Then, the output signal of the photo-detector measured by the phasemeter introduces a clock noise δL_c, due to the fluctuations from the USO. Next, the error signal L_e is obtained by using a linear combination of two different phasemeters output, where the symbols L_+ represents the sum of two interfering arm's signals and L_- represents the difference between the two interfering arms' signals, so the transfer function of the dual arm-locking sensor can be written as

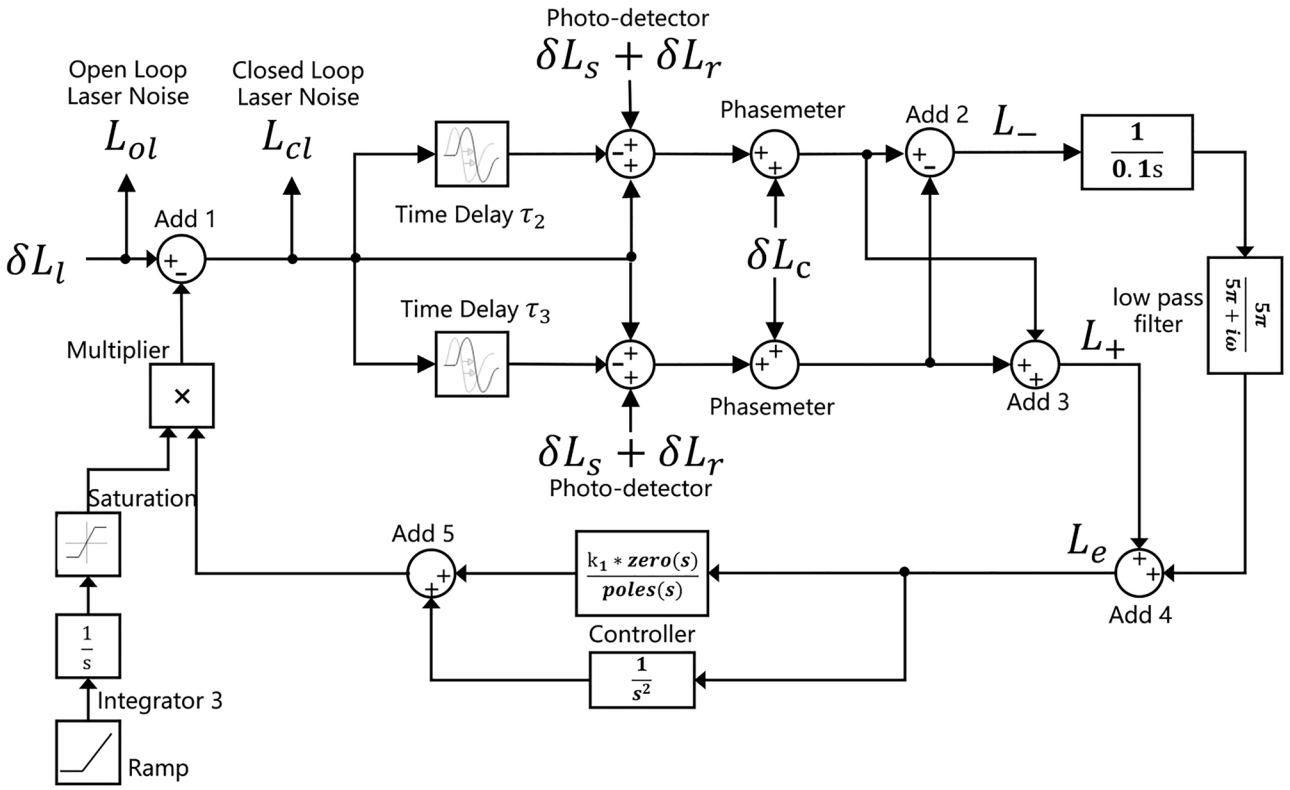

Fig. 9 The Simulink model of dual arm-locking

Table 3 Parameter values for the time domain simulation

Simulation Parameter	Value
Time delay τ_2	20 s
Time delay τ_3	20.2 s
Gian k_1	10
Ramp signal slope	0.001
Ramp signal start time	30 s
Simulation time	11 000 s

$L_e(s) = L_+(s) + E(s)/\Delta\tau s \cdot L_-(s)$. At last, the error signal is filtered by the controller and then feedback controls the laser. The filter controller of the dual arm-locking also consists of a compensation filter and two-stage integrators in parallel, of which the controller configuration is the same as that of the single arm-locking. The parameter values of the controller are listed in Table 1 and the bode plot is shown in Fig. 4. In the entire model loop of the dual arm-locking system, the variable is the displacement and four different noises shown in the noise levels section.

Simulation Results

When the dual arm-locking began, the open loop and closed loop laser noises were both measured for 11 000 s, and the data for the first 1 000 s were removed to reduce the turn on transient effects. Fig. 10 shows the ASD of the laser displacement noise before and after dual arm-locking, where the blue trace is the open loop laser noise and the red trace is the closed loop laser noise. The simulation results show that the laser noise of closed loop after dual arm-locking was lower than 3.19 μm/$\sqrt{\text{Hz}}$@10 mHz in the frequency range of 0.1 mHz – 1 Hz, meeting the requirement of Taiji mission.

From Fig. 8 and Fig. 10 it can be concluded that under the same configuration of the filter controller, dual arm-locking has better laser noise suppression performance than that of the single arm-locking, and no nulls appear in a frequency range of 0.1 mHz – 1 Hz. Besides, it is also worth noting that the simulation results didn't represent the limit of the ability of noise suppression of arm-locking technology. The laser noise suppression performance could be improved by optimizing the controller parameters.

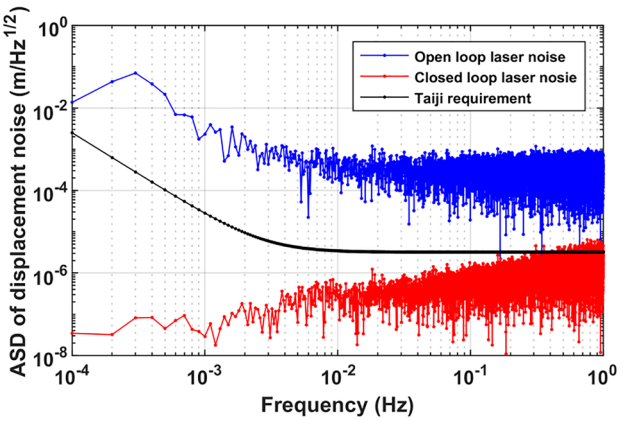

Fig. 10 The ASD of the laser noise before and after dual arm-locking

Conclusions

Some simulation results of arm-locking were presented in this paper, which represented a significant step forward in demonstrating the arm-locking suitable for the Taiji mission. An innovative controller consisted of a compensation filter and two-stage integrators in parallel adopted in the paper can suppress the laser frequency noise without increasing gain and prevent the high gain from suppressing the gravitational waves signal. The simulation results showed that the single arm-locking system could reduce the laser frequency noise to lower than 3.19 μm/$\sqrt{\text{Hz}}$@10 mHz in the frequency range of 0.1 mHz – 0.03 Hz. However, there were a few nulls in the frequency range of 50 mHz – 1 Hz, which made it inadaptable for the Taiji mission. Compared to the single arm-locking, the dual arm-locking system can overcome the nulls, which can suppress the laser frequency noise to lower than 3.19 μm/$\sqrt{\text{Hz}}$@10 mHz in the full frequency range of 0.1 mHz – 1 Hz, meeting the requirement of Taiji mission. Next step, the Doppler shift and the heterodyne weak-light phase-locking will be introduced into the simulation model to study the impact of the frequency pulling on the arm locked laser, and on-ground laser arm-locking demonstration by using an electronic phase delay device will be investigated.

Acknowledgements This work was supported by the Youth Innovation Promotion Association, Chinese Academy of Sciences, Grant No.2018024, and the National Science Foundation of China, Grant No.61575209, and the Strategic Priority Research Program of the Chinese Academy of Sciences, Grant No. XDB23030200.

References

Abbott, B.P., Abbott, R., Abbott, T., Abernathy, M., Acernese, F., Ackley, K., Adams, C., Adams, T., Addesso, P., Adhikari, R.: GW151226: observation of gravitational waves from a 22-solar-mass binary black hole coalescence. Phys. Rev. Lett. **116**(24), 241103 (2016a)

Abbott, B.P., Abbott, R., Abbott, T., Abernathy, M., Acernese, F., Ackley, K., Adams, C., Adams, T., Addesso, P., Adhikari, R.: Observation of gravitational waves from a binary black hole merger. Phys. Rev. Lett. **116**(6), 061102 (2016b)

Abbott, B.P., Abbott, R., Abbott, T.D., Acernese, F., Ackley, K., Adams, C., Adams, T., Addesso, P., Adhikari, R., Adya, V.: GW170817: implications for the stochastic gravitational-wave background from compact binary coalescences. Phys. Rev. Lett. **120**(9), 091101 (2018)

Abramovici, A., Althouse, W.E., Drever, R.W., Gürsel, Y., Kawamura, S., Raab, F.J., Shoemaker, D., Sievers, L., Spero, R.E., Thorne, K.S.: LIGO: The laser interferometer gravitational-wave observatory. science **256**(5055), 325–333 (1992)

Acernese, F., Antonucci, F., Aoudia, S., Arun, K., Astone, P., Ballardin, G., Barone, F., Barsuglia, M., Bauer, T.S., Beker, M.: Performances of the Virgo interferometer longitudinal control system. Astropart. Phys. **33**(2), 75–80 (2010)

Ando, M., Kawamura, S., Seto, N., Sato, S., Nakamura, T., Tsubono, K., Takashima, T., Funaki, I., Numata, K., Kanda, N.: DECIGO and DECIGO pathfinder. Class. Quantum Gravity **27**(8), 084010 (2010)

Arain, M.A., Mueller, G.: Design of the Advanced LIGO recycling cavities. Opt. Express **16**(14), 10018–10032 (2008)

Beker, M., Blom, M., van den Brand, J., Bulten, H.J., Hennes, E., Rabeling, D.: Seismic attenuation technology for the Advanced Virgo gravitational wave detector. Physics Procedia **37**, 1389–1397 (2012)

Black, E.D.: An introduction to Pound–Drever–Hall laser frequency stabilization. Am. J. Phys. **69**(1), 79–87 (2001)

Cornish, N.J.: Detecting a stochastic gravitational wave background with the Laser Interferometer Space Antenna. Physical Review D **65**(2), 022004 (2001)

Cyranoski, D.: Chinese gravitational-wave hunt hits crunch time. Nature **531**(7593), 150–151 (2016)

Danzmann, K., Prince, T., Binetruy, P., Bender, P., Buchman, S., Centrella, J., Cerdonio, M., Cornish, N., Cruise, M., Cutler, C.J., Finn, L.S., Gundlach, J., Hogan, C., Hough, J., Hughes, S.A., Jennrich, O., Jetzer, P., Lobo, A., Madau, P., Madau, Y., Phinney, S., Richstone, D.O., Schutz, B., Stebbins, R., Sumner, T., Thorne, K., Vinet, J.Y., Vitale, S.: LISA: Unveiling a hidden Universe. Assessment Study Report ESA/SRE (Yellow Book). In. Tech. Rep, (2011)

de Vine, G., Ware, B., McKenzie, K., Spero, R.E., Klipstein, W.M., Shaddock, D.A.: Experimental Demonstration of Time-Delay Interferometry for the Laser Interferometer Space Antenna. Physical Review Letters **104**(21) (2010). doi:https://doi.org/10.1103/PhysRevLett.104.211103

Dong, Y., Liu, H., Luo, Z., Li, Y., Jin, G.: A comprehensive simulation of weak-light phase-locking for space-borne gravitational wave antenna. Science China Technological Sciences **59**(5), 730–737 (2016)

Gair, J.R., Vallisneri, M., Larson, S.L., Baker, J.G.: Testing general relativity with low-frequency, space-based gravitational-wave detectors. Living Rev. Relativ. **16**(1), 7 (2013)

Grote, H., Collaboration, L.S.: The GEO 600 status. Class. Quantum Gravity **27**(8), 084003 (2010)

Hu, W., Wu, Y.: The Taiji Program in Space for gravitational wave physics and the nature of gravity. In. Oxford University Press, (2017)

Hughes, S.P.: General method for optimal guidance of spacecraft formations. Journal of guidance, control, and dynamics **31**(2), 414–423 (2008)

Kawamura, S., Nakamura, T., Ando, M., Seto, N., Tsubono, K., Numata, K., Takahashi, R., Nagano, S., Ishikawa, T., Musha, M.: The Japanese space gravitational wave antenna—DECIGO. Class. Quantum Gravity **23**(8), S125 (2006)

Luo, J., Chen, L.S., Duan, H.Z., Gong, Y.G., Hu, S.C., Ji, J.H., Liu, Q., Mei, J.W., Milyukov, V., Sazhin, M., Shao, C.G., Toth, V.T., Tu, H.B., Wang, Y.M., Wang, Y., Yeh, H.C., Zhan, M.S., Zhang, Y.H., Zharov, V., Zhou, Z.B.: TianQin: a space-borne gravitational wave detector. Classical And Quantum Gravity **33**(3), 19 (2016). https://doi.org/10.1088/0264-9381/33/3/035010

Luo, Z., Wang, Y., Wu, Y., Hu, W., Jin, G.: The Taiji program: A concise overview. Progress of Theoretical and Experimental Physics (2020)

McKenzie, K., Spero, R.E., Shaddock, D.A.: Performance of arm locking in LISA. Physical Review D **80**(10), 102003 (2009)

Pitkin, M., Reid, S., Rowan, S., Hough, J.: Gravitational wave detection by interferometry (ground and space). Living Rev. Relativ. **14**(1), 5 (2011)

Robertson, D., Hough, J.: Interferometry for LISA. Class. Quantum Gravity **13**(11A), A271 (1996)

Scientific, L., Abbott, B., Abbott, R., Abbott, T., Acernese, F., Ackley, K., Adams, C., Adams, T., Addesso, P., Adhikari, R.: GW170104: observation of a 50-solar-mass binary black hole coalescence at redshift 0.2. Physical Review Letters **118**(22), 221101 (2017)

Sheard, B.S., Gray, M.B., McClelland, D.E., Shaddock, D.A.: Laser frequency stabilization by locking to a LISA arm. Phys. Lett. A **320**(1), 9–21 (2003). https://doi.org/10.1016/j.physleta.2003.10.076

Sheard, B.S., Gray, M.B., Shaddock, D.A., McClelland, D.E.: Laser frequency noise suppression by arm-locking in LISA: progress towards a bench-top demonstration. Class. Quantum Gravity **22**(10), S221–S226 (2005). https://doi.org/10.1088/0264-9381/22/10/013

Sutton, A., Shaddock, D.A.: Laser frequency stabilization by dual arm locking for LISA. Physical Review D **78**(8), 082001 (2008). https://doi.org/10.1103/PhysRevD.78.082001

Thorpe, J.I., Cruz, R.J., Sankar, S., Mueller, G.: Electronic phase delay—a first step towards a bench-top model of LISA. Class. Quantum Gravity **22**(10), S227 (2005)

Thorpe, J.I., McKenzie, K.: Arm locking with the GRACE follow-on laser ranging interferometer. Physical Review D **93**(4), 042003 (2016). https://doi.org/10.1103/PhysRevD.93.042003

Thorpe, J.I., Mueller, G.: Experimental verification of arm-locking for LISA using electronic phase delay. Phys. Lett. A **342**(3), 199–204 (2005). https://doi.org/10.1016/j.physleta.2005.05.053

Tröbs, M., Heinzel, G.: Improved spectrum estimation from digitized time series on a logarithmic frequency axis. Measurement **39**(2), 120–129 (2006)

Wang, G., Ni, W.-T.: Numerical simulation of time delay interferometry for TAIJI and new LISA. Research in Astronomy and Astrophysics **19**(4), 058 (2019)

Willke, B., Aufmuth, P., Aulbert, C., Babak, S., Balasubramanian, R., Barr, B., Berukoff, S., Bose, S., Cagnoli, G., Casey, M.M.: The GEO 600 gravitational wave detector. Class. Quantum Gravity **19**(7), 1377 (2002)